Dynamics of a Compliant Membrane as Related to Mammalian Flight

Arnold J. Song* and Kenneth S. Breuer†

Brown University, Providence, RI 02912, USA

Bats and other mammalian gliders exhibit extraordinary flight capabilities some of which are attributable to their unique wing structure which is quite distinct from birds and insects. In mammalian flight, the wing is composed of a thin compliant membrane of skin which has the ability to adapt to flow conditions. In an effort to characterize the distinctive aerodynamics of compliant membrane wings, results from wind tunnel tests of the static deformation and unsteady vibrations of a low aspect ratio wing are presented. The unsteady deflection of a latex membrane model was measured via high-speed, stereo photogrammetry. The tested wing has a half-span aspect ratio of 0.69 and experiments were performed with two pretensioned configurations: (1) 0 % prestrain and (2) 5 % prestrain. Testing was performed at angles of attack ranging from $4-34^\circ$ and $Re_c = 60,000-140,000$. The static normalized camber versus angle of attack, or camber slope, was found to decrease with increasing Reynolds number. In addition, high order vibrational modes were observed to occur in a range of angles of attack ($\alpha = 16-28^\circ$) above a critical value of the Reynolds number ($Re_c > 80,000$). Fourier analysis of these membrane vibrations show that the dominant frequencies fall along distinct bands of slightly decreasing reduced frequency.

Nomenclature

c	Chord length
Δc	Elongation length
k	Membrane spring constant
k	Reduced frequency
x	Chordwise coordinate
y	Spanwise coordinate
z	Chord-normal coordinate
$z*$	Camber normalized by chord length
F_n	Chord-normal force
T	Tension
β	Deflection angle, i.e. angle between membrane and chordline

I. Introduction

Low Reynolds number, low aspect ratio (LAR) aerodynamics is an area of increased research activity, driven in large part by the recent interest in unmanned, small-sized aircraft, or micro air vehicles (MAVs), with desired dimensions of the order of a 15-cm wingspan at 5-20 m/s.[1] In addition there is growing interest in the experimental and computational study of flight in insects, birds and bats.[2–5] The utilization of LAR wings composed of thin, yet tough skin membrane is seen primarily in flying and gliding mammals, such as bats, flying squirrels and sugar gliders.[6,7] These mammalian flyers can exhibit extraordinary flight agility and maneuverability which is contributed to in part by the utilization of a compliant membrane as the lifting

*Graduate Student, AIAA Student Member

†Professor, AIAA Senior Member

surface. In contrast, the structure of avian wings have thicker airfoil sections and are comparatively more rigid than the mammalian wings,[8] while on the lower end of the Reynolds number spectrum of biological flyers, insect flight can be characterized as the relatively simple flapping of rigid, yet aerodynamically thin airfoils.[9] The membrane lifting surface is supported by a skeletal "airframe" capable of a high degree of articulation (from the shoulder and elbow, but particularly the wrist and finger which shape the outboard portion of the wing)[10] which is enabled by the very flexible and pliable membrane. This unique structure of the mammalian flyers' wings suggests that further study of the aerodynamics and biomechanical mechanisms in these animals may provide useful information and inspiration for the design of compliant membrane MAVs.

Figure 1. Bat in flight. Note the large degree of camber in the wing. The unique aerodynamic properties of a compliant membrane wing are believed to play significant role in the high degree of maneuverability exhibited by bats in flight. The skeletal structure of the bat wing allows for considerable articulation of the outboard portion of the wing. Photo courtesy of the Lubee Foundation

A challenging aspect of the study of mammalian flight is the inherently unsteady nature of flapping flight and the intermediate Reynolds number where many complex aerodynamic phenomena, such as transition to turbulence and laminar separation, are both present and hard to predict. Although this area of aerodynamics has not been studied extensively, there are some notable exceptions in recent years.[11,12]

On the experimental front, studies by Torres and Mueller have examined several planforms of rigid LAR wings. Torres and Mueller suggest that the large non-linearities in the lift curves for wings with aspect ratios less than 1.25 are due to wing tip vortices.[12] These flow structures contribute to an increased maximum lift, $C_{L_{max}}$, and the delay of stall to a larger angle of attack. The interaction of the wingtip vortices with the flow over the lifting surface for LAR wings is analogous to the delta wing, which has vortex lift at high angles of attack.

Very recent efforts by Tian and coworkers[13] have examined the aerodynamics of LAR compliant membrane wings over a range of Reynolds numbers, $Re_c = 70,000 - 180,000$ for a wing with half-span aspect ratios ranging from 0.46 to 0.69. As compared to the rigid wing, the compliant membrane exhibits superior lift performance. In addition, the adaptive cambering mechanism of the compliant membrane wing attenuates the severity of the stall condition resulting in a "softer" decrease in lift after the onset of stall. Lastly, significant lift curve hysteresis was observed in which finite lift forces were obtained for very low non-zero angles of attack.

Motivated by nature's flyers, MAV designers have recognized the potential of flexible membrane wings to achieve improved agility and efficiency, and some recent designs of MAVs have utilized membrane wings because of their adaptive-wing structure.[14] These designs look to the successful and highly maneuverable flight of bats as the source of inspiration for their vehicles despite the lack of a clear understanding of the physical mechanisms at play. As MAV design has progressed, little basic science research has attempted to develop a comprehensive model of the fluid-structure interaction contributing to the improved performance of flexible membrane flyers. The ability of a compliant membrane wing to passively adapt to changing flow conditions may prove to be a powerful tool in MAV and low Reynolds number air vehicle design. In particular, the adaptive camber mechanism of compliant membrane wings may result in superior gust alleviation as compared to rigid wings. However, without experimental studies of compliant membrane aerodynamics the design process remains in a trial and error mode of operation.

The study of the full complexity of mammalian flight is challenging but is nevertheless underway.[5] However, a significant challenge in working with live animals is the requirement that the testing must be accomplished in a safe and humane manner, and furthermore, that it is difficult, if not impossible, to isolate unique contributions that different characteristics of an animal's morphology contribute to its overall aerodynamic performance.

To address these issues, we have thus embarked on a systematic study with an attempt to isolate different morphological features present in mammalian flight and to explore the role that each plays. While Tian et al.[5,13] measured lift and drag characteristics. the current study focuses on the geometric behavior of thin membrane wings and on the dynamics of the membrane as it is subjected to aerodynamic loads. A simple

low aspect ratio membrane wing is tested in a low-speed wind tunnel over a range of (low) Reynolds numbers and angles of attack. We have measured the three-dimensional shape of the wing as it deforms while subject to aerodynamic loading. This is accomplished using high-speed, stereo photogrammetry which allows us to measure not only the static deflection of the wing but also the onset of unsteady wing motions.

The series of experiments presented in this paper are a continuation of preliminary results reported by Galvao and coworkers.[15] In the previous work, the stiffness of the membrane was varied by the variation of the membrane thickness. The experiments presented in this paper explore the importance of tension in the membrane dynamics. In addition, the aspect ratio is nearly 1.5 times that of the previous model to begin to look at the interplay between the lift generated by potential flow and tip vortices.

II. Analytical Considerations

The interplay between membrane tension and aerodynamic loads result serves as a feedback mechanism which enhances the adaptive cambering of the membrane. The aerodynamic loads induced by the membrane wing cause the complaint membrane to stretch therefore increasing the membrane tension to counteract these loads. This elongation of the membrane due to aerodynamic loading increases the camber which then increases the lift and drag generated by the wing. This feedback between the aerodynamic forces, membrane camber, and membrane tension continues until an equilibrium is reached between the membrane tension and aerodynamic loads. Therefore, the equilibrium shape of the wing, which will be primarily characterized by the magnitude of the camber for these small deformations, is dependent upon the tension established by the stretching of the membrane and the angle that the membrane makes with the camber line at the leading and trailing edges (β_{LE} and β_{TE}), which will be referred to as the *deflection angle*. The aerodynamic load on the membrane is the component of the resultant force which is normal to the camber line, F_n. Since this force must be equal to the component of the membrane tension which is also normal to the chordline, we can then express the aerodynamic loading in terms of the membrane tension and deflection angle:

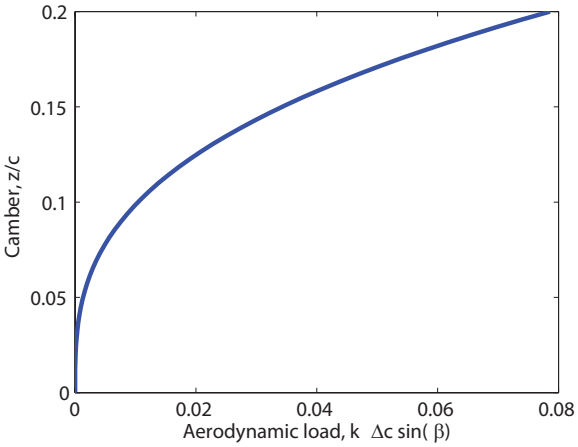

Figure 2. Camber versus aerodynamic loading. Due to the diminutive value of the deflection angle β for small values of camber the camber increases rapid for small aerodynamic loads. As the camber increases, the increase in membrane stiffness and deflection angle requires larger increments of aerodynamic loading to achieve the same increase in camber seen initially.

$$F_n = T(\sin(\beta_{LE}) + \sin(\beta_{TE})) \tag{1}$$

where the tension in the membrane is denoted as T. If the deflection angles at the leading and trailing edges are assumed to be very nearly equal then the equalizing force in the membrane reduces to

$$F_n \approx 2T\sin(\beta) \tag{2}$$

and

$$T = k\Delta c \tag{3}$$

where k and Δc are the membrane spring constant and elongation respectively.

To shed some light on the cambering mechanism at play in the compliant membrane wing, we present a simple model of a membrane subjected to aerodynamic loading. The camber line, $z(x)$, is approximated as a quadratic function of chordwise coordinate, x: $z(x) = 4z_{max}x(1-x)$. In addition, the membrane is approximated to behave like a linear, Hookean spring, i.e. the spring coefficient k in Eq.(3) is taken to be constant. In the model presented in this paper, the membrane spring constant is taken to be $k = 1$. In reality, both biological and man-made membranes are known to exhibit nonlinear J-shaped stress-strain behaviors in which k increases with extensions. This behavior is ignored for the current analysis.

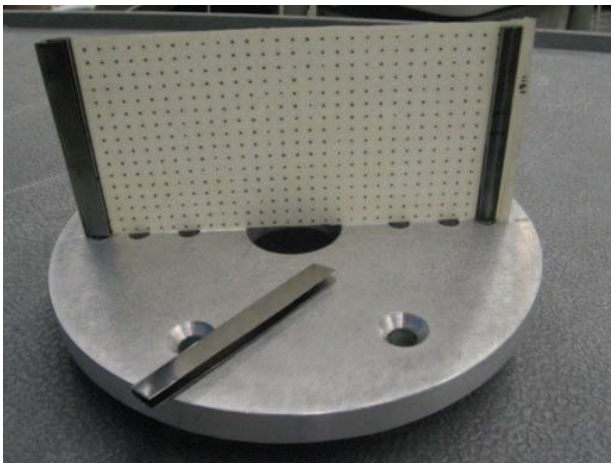

(a) Compliant membrane model used in wind tunnel testing. For the series of experiments presented in this paper, an array of 340 markers were tracked. DLT was used to map the stereo image plane marker locations to their respective three-dimensional real space coordinates.

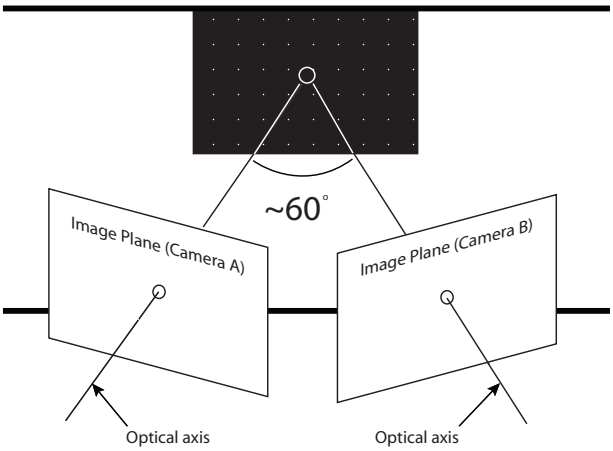

(b) Schematic of stereophotogrammetry setup. When possible the angle between the cameras was approximately 70°. However, the geometry of the wind tunnel test section did not allow for this separation angle for large angles of attack.

Figure 3. Experimental setup.

Combining these equations results in a simple prediction for the maximum camber, z_{max}, as a function of the aerodynamic load, $F_c \approx k\Delta c \sin(\beta)$, shown in Fig.2. We see from Eq.(2) that even if the tension of the membrane is very large, the membrane does not provide any resistance to deflection for small values of βT ($\sin\beta \approx \beta$). Therefore, the camber increases rapidly for the initially small values of β corresponding to small aerodynamic loads. Eventually, as seen in Fig. 2 the membrane reaches a region where the increase in camber is relatively small with large increases in the loading. However, if the initial tension in the membrane is large, the rapid initial rise in the camber will be more subdued. Increasing the membrane stiffness will also dampen the cambering behavior.

III. Experimental Procedure

A. Compliant Membrane Models

A compliant membrane wing was designed and manufactured for the experiments. The details of the constructions are similar to that used in previous experiments by our group,[5,15] and summarized here for convenience. The rectangular wing is composed of a compliant latex membrane held between two stainless steel posts located at the leading and trailing edges (Fig. 3(a)). The posts measure 9.0 cm in height and are secured to an aluminum mounting plate designed to attach to the force balance which is mounted on the test section ceiling. At either end of wing, the membrane material is inserted through a slit aligned with the centerline of the post then secured using spring steel clamps. With the clamps in place, the leading and trailing edges are approximately parabolic in shape with a maximum thickness of 3.7 mm. The fully assembled wing measures 12.9 cm (chord, c) by 9.0 cm (half-span, b), giving a half-wing aspect ratio of 0.69.

Two configurations were considered in this series of experiments:

- 0% prestrain: Membrane is mounted in its relaxed state.
- 5% prestrain: Membrane is elongated by 5% of its original length.

B. Stereo Photogrammetry

A stereo photogrammetry system was developed to measure the instantaneous deflection of the wing. Two high-speed CMOS cameras (Photron PCI-1024) were placed outside the wind tunnel test section with an approximate 70° angle of separation between their respective optical axes. For higher angles of attack (above 25°) the camera separation angle was reduced to 60° and the cameras moved closer to one another to be able to maintain the ability to discern markers across the wing membrane at these high angles. The cameras

have a pixel resolution of 1024 x 1024, which in conjunction with the imaging optics (Nikon 60 mm Micro Nikkor lenses) provided a spatial resolution of 0.20 mm per pixel. For this series of experiments, the unsteady motion of the membrane was recorded for 1.0 seconds at 1000 Hz (1000 frames) at each speed and angle of attack.

Custom software, utilizing direct linear transformation (DLT),[16] was used to recover the coordinates of each marker location in the 3D object space from two 2D images at each time step. A calibration cube consisting of a three-dimensional grid of markers was used to generate the calibration coefficients needed to reconstruct coordinates in the object space via DLT. The measurement uncertainty of displacement measurements using the DLT method is less than $\pm 35\mu$m for in plane displacements and $\pm 40\mu$m for out of plane displacements, with the reference plane taken to be the plane coincident with the undeflected geometry of the membrane.

IV. Results and Discussion

A. Static Behavior

The compliant membrane wing is unique because of its ability to adaptively change shape in response to changing flow conditions. This also means that the membrane is sensitive to slight variations in the flow about the wing such as periodic vortex shedding, slight perturbations of the pressure distribution, etc. Therefore, the membrane wing is in constant motion. However, if the deviations from the mean shape are small then we can assume that the lift and drag generated by the membrane wing is due to its time-averaged geometry. The static shape of the membrane wing, (Fig.4) is generated from the mean individual marker coordinates of the marker array over the acquisition time (1000 frames over 1 second).

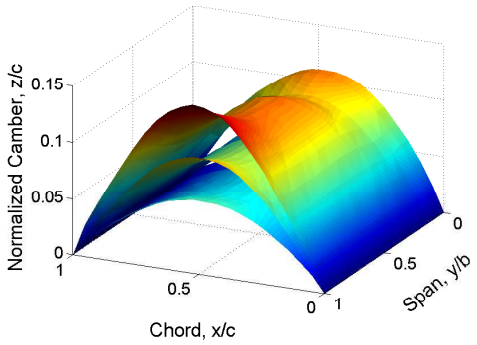

Figure 4. Static deformation of a compliant membrane wing due to aerodynamic loading. The membrane geometry is shown for $\alpha = 24°$, $Re_c = 70,104$, and 140×10^3. The static surface geometry of the membrane is obtained from the time-averaged position of marker array. Note that the deflection of the membrane tip is greater than the root deflection.

First, we will consider the static deformation of a compliant membrane with no initial tension. Fig. 5(a) illustrates how the maximum camber normalized by the dynamic pressure ($q = 1/2\rho U^2$) varies with the angle of attack. At a constant Reynolds number, the camber increases with angle of attack until reaching a maximum between $\alpha = 20 - 22°$ indicating the onset of stall. As the degree of flow separation increases, the magnitude of maximum camber begins to level off and then slowly decreases. This behavior is quite consistent with the lift characteristics of compliant wings measured by Tian et al.[13] It is also observed that the regime in which the camber levels off and then decreases occupies an increasingly wider range of angles of attack with increasing Reynolds number. The relationship between the maximum camber normalized by the dynamic pressure versus angle of attack, which will be referred to as the *camber slope*, is not constant over the range of Reynolds number considered in these experiments. In fact, we see that the camber slope decreases with increasing Reynolds number.

When the dynamic pressure is low (low values of Re), the camber normalized by the dynamic pressure has a stronger dependence on angle of attack than for higher magnitudes of dynamic pressure. For low dynamic pressure, the membrane deflection is relatively small. These small values of membrane deflection result in modest values of the deflection angle, therefore the membrane must elongate even more to achieve the combined tension and deflection angle necessary to balance the aerodynamic load (see Eq.(2)). As the membrane deflection increases, the combination of the deflection angle and elongation results in a greater resistance to further cambering. The decrease in the camber slope with increasing dynamic pressure is due to this combined effect of an increase in tension (elongation) and increase in deflection angle due to membrane cambering. This is most pronounced at $Re = 60,000$ and $86,000$ where a slight "bend" in the camber slope as the angle of attack is increased.

As the Reynolds number is increased (also increased dynamic pressure) the rapid increase in the membrane camber occurs over a smaller range of angles of attack which is manifested in an apparent initial "jump" in the camber at low angles of attack, e.g. $Re = 112,000$ in Fig. 5(a), after which the camber slope is

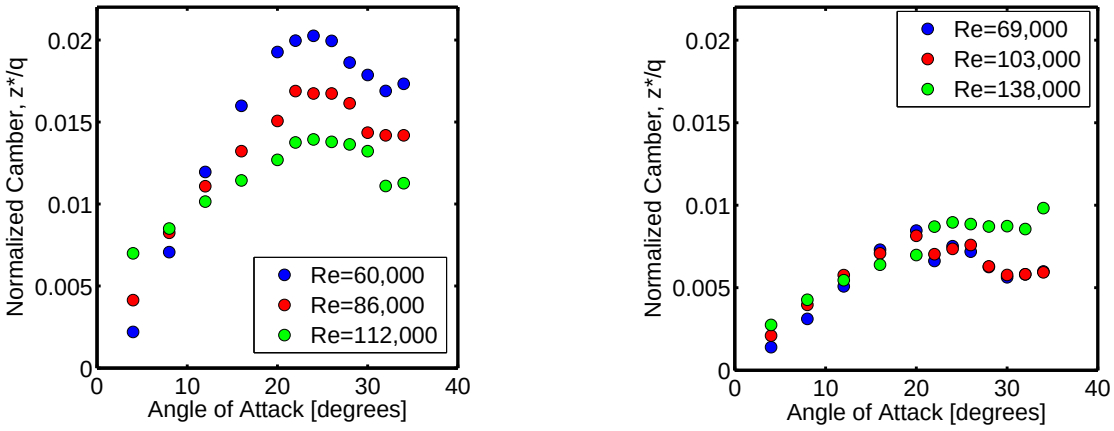

(a) 0% prestrain

(b) 5% prestrain

Figure 5. Maximum camber as function of angle of attack for unstrained and pre-strained wings. Note that in both cases, the camber does not scale with dynamic pressure, due to the effects of both the nonlinear stress-strain characteristics of the membrane material as well as the geometry of cambering wings.

nearly constant. The slight decrease in camber slope with increasing values of α observed for lower Reynolds number camber curves is not seen in this higher Reynolds number case. Since, the magnitude of the lift and drag induced by the membrane wing is much higher at this Reynolds number even for low values of angle of attack, a significantly greater degree of camber is needed to balance these aerodynamic loads. The observed jump can be explained as an artifact of the resolution of the experimental parameter space which does not capture this rapid rise in camber at angles of attack between $\alpha = 0 - 4°$.

For the membrane which has been pretensioned (5% prestrain), the magnitude of the camber is significantly reduced for the corresponding angles of attack and Reynolds number in constrast to the zero pretension case. This is expected since there is more resistance to elongation for a given applied force. Additionally, the initial elongation of the membrane changes the stress-strain regime in which the material is operating. While the previous, non-prestrained, case operates within a nonlinear regime which then reaches an asymptotic value of the elastic modulus, this prestrained case operates entirely within the linear regime. Therefore, for this prestrained case, the nonlinearity of the membrane elasticity has little influence on its cambering behavior.

We know from Eq.(2) that the membrane behavior of the pretensioned case (5% prestrain) should follow the same general pattern of the untensioned configuration. We see that the camber slope does indeed decrease with increasing Reynolds number as with the 0% prestrain case albeit with a much smaller variation. It is the relatively large initial tension which allows the membrane to equalize the aerodynamic loads for smaller values of the deflection angle because it is the product of the membrane tension and the deflection angle β which determines the magnitude of the aerodynamic load that the membrane can counteract.

We have identified two coupled, nonlinear mechanisms which describe the cambering behavior of low aspect ratio membrane wings:

- The camber reenforcing property of a lifting surface composed of a compliant material.
- Nonlinearity of the stress-strain relationship at low values of stress.

For an airfoil operating in the pre-stall regime, an increase in the angle of attack will result in the increase in the pressure differential between the upper and lower surfaces, i.e. the resultant aerodynamic forces (lift and drag). Typically, the lift is linearly dependent on the angle of attack. In contrast to a rigid wing, a compliant membrane will elongate and increase the camber of the wing as the aerodynamic loads increase which further increase these aerodynamic loads. As the membrane elongates, the tension in the membrane and the deflection angle are also increasing. Eventually, the wing will attain a quasi-steady state where the applied aerodynamic force and the tension of the membrane are balanced.

The nonlinearity of the elastic modulus of the latex membrane used in this experiment also plays a role in the cambering behavior. For 0% prestrain, the membrane is operating in a highly nonlinear stress-strain

regime. This nonlinearity further enhances the effects of the membrane's camber enhancing mechanism, allowing the membrane to strain to a higher degree for low values of stress until reaching an asymptotic state of a nearly linear stress-strain relationship at larger extensions.

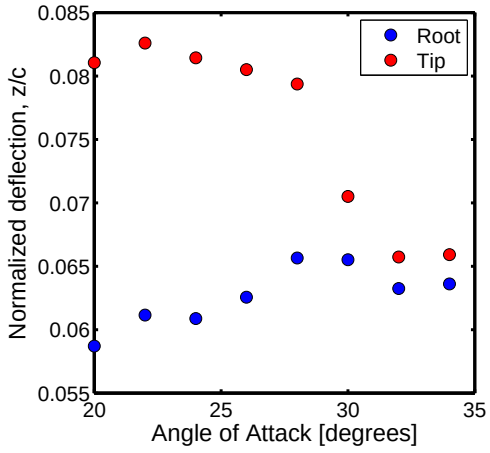

Figure 6. Comparison of Tip and Root Deflection. The influence of the tip vortex is particularly strong at low angles of attack, but diminishes at stall.

A key component of the favorable lift characteristics of a low aspect ratio wing is the influence of tip vortices over a greater portion of the wing. These tip vortices generate low pressure regions over a significant portion of the wing, a phenomenon distinct from wings with larger aspect ratios where these same tip vortices are confined to a smaller proportion of the lifting surface. Thus, for LAR wings, a greater fraction of the lift is generated via tip vortices. In addition, the downwash from the tip vortices provides the chord-normal momentum needed for the flow to remain attached, thereby allowing a LAR wing to operate at higher angles of attack than would be possible for a wing of higher aspect ratio at these moderate values of Reynolds number ($Re \approx 60 - 130 \times 10^3$).[12]

For this series of experiments, the tip and root of a half span model are unconstrained while the leading and trailing edges are fixed, as seen in Fig. 4. The shape of the membrane provides a window into the pressure distribution over the wing. In particular, we observe a significant difference between the deflections at the root and tip (Fig. 6), and this differential qualitatively indicates the strength and extent of the tip vortex, and its influence on the inboard portion of the wing. However, as the angle of attack rises, the presumed growth of a laminar separation bubble will generate a low pressure region which in turn will weaken the tip vortex. The combination of the decrease in vortex strength and core size translates into the diminished contribution of vortex lift to the overall lift of the wing. We see this reflected in the relative deflections of the tip and root in Fig. 6. Prior to stall, the LAR wing begins to experience a decrease in lift slope corresponding to a change in the geometry. The inboard camber continues to increase due presumably due to the continually increasing potential lift and drag. However, as the angle of attack is increased even further, the tip deflection begins to decrease or deflate corresponding to the weakening of the tip vortex. This deflation of the tip continues with increasing angle of attack until a severe drop in the tip deflection occurs. This is postulated to be correspondent to the bursting of the tip vortex and full on separation of the flow over the rest of the wing at which point the wing geometry is nearly two dimensional where the tip and root deflections are essentially one and the same. These conjectures need to be confirmed with more detailed flow measurements - an experiment planned for the near future.

B. Dynamic Behavior

Complementary to the static measurements of the camber and shape of the membrane, the dynamic behavior of the LAR membrane wing was also characterized. The leading edge of the wing configuration is assumed to be sharp enough to induce the formation of leading edge vortices, at sufficiently high angles of attack, which are periodically shed downstream. The vibrations of the membrane are believed to be due to the shedding of these vortical structures along the chordwise direction of the membrane and a result of the flutter at the wingtip. The periodicity of the vortex shedding results in distinct spatial modes of vibrations (Fig. 7). These mode shapes correspond closely to the eigenmodes ("drum modes") of a membrane subject to Dirichlet boundary conditions at leading and trailing edges and Neumann boundary conditions at the tip and root.

We have constructed a phase map of the harmonic order providing a qualitative picture of the vibrational modes of the membrane. As seen in Fig. 8, the higher modes of vibration are excited beyond a critical Reynolds number of approximately 80,000 within a band of angles of attack between $16 - 28°$. The confinement of the higher eigenvalue modes to this range of Reynolds number and angle of attack suggest that resonance between the membrane and the flow is occurring in this range. In addition, this resonance occurs in the range of angle of attack in which the flow is beginning to separate which can been inferred

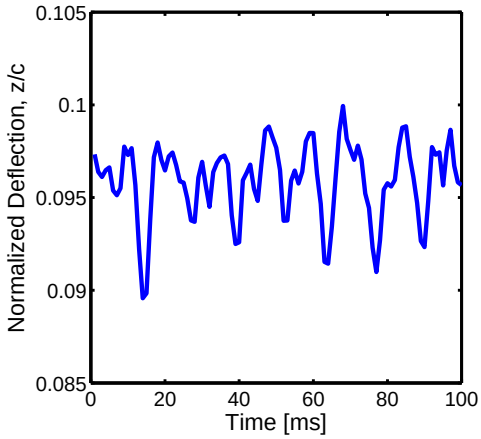

(a) Time trace of marker camber-normal (z) movement.

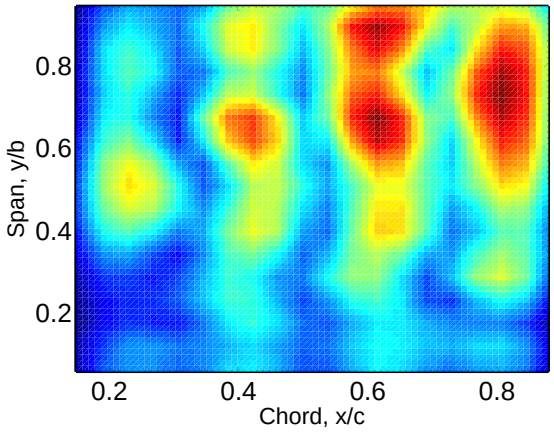

(b) Plot of RMS magnitude for $\alpha = 28°$, $Re_c = 120,000$.

Figure 7. Unsteady vibration of compliant membrane, temporal and spatial structures.

from the levelling off of the magnitude of the camber for this range of angle of attack.

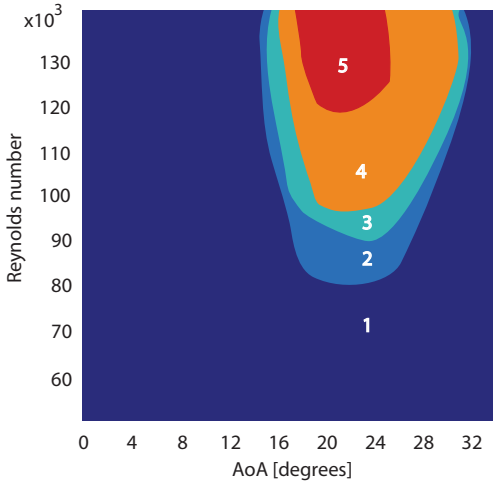

Figure 8. Phase map of membrane drum modes (eigenmodes). The number indicate the number of peaks observed in the RMS magnitude structure. The colored regions denote the interpolated regions which each mode (corresponding to number of peaks) resides.

In contrast to the results of Galvao et al.,[15] where the RMS magnitudes were nearly uniform in the spanwise direction, the higher magnitudes of the RMS values, i.e. the stronger vibrations, tend to be proximal to the tip. This is believed to be a result of the more than 50% increase in the aspect ratio which results in a decrease of the proportion of the wing which is influenced by the tip vortices. This suggests that at near-stall angles of attack, the tip flutter induced by flow leakage from the lower to upper surface may be the source of vibrational forcing, while the leading edge vortex shedding may in fact be dampening these vibrations which results in the lower magnitudes of RMS in the inboard region.

Fourier analysis of the unsteady deflections was performed to determine the most significant frequency of the vibrations. The ensemble average of the power spectra of the marker array is used to obtain results for each angle of attack. For each angle of attack, we have constructed a waterfall diagram for the membrane vibrational behavior, as seen in Fig. 9 for $\alpha = 24°$. At each Reynolds number, a power spectrum was obtained and plotted versus the reduced frequency ($k = fc/U$). The width of each of the power spectra is uniform and arbitrary and serves only for clarity of presentation. From this result at $\alpha = 24°$, we see that the dominant reduced frequencies, $k = fc/U$, fall along well-defined bands at discrete values of k that decrease slightly with increasing Reynolds number. This trend in the peak reduced frequencies suggests that the frequency of the vortex shedding from the leading edge may not directly proportional to wind speed. The influence of downwash from the tip vortex which may provide enough chord-normal momentum to attenuate the shedding from the leading edge resulting a reduction in the shedding frequency. The maximum energy shifts to higher values of k as Re increases confirming that higher membrane modes are being excited at the higher speeds. However, the details of the underlying mechanism that generate this banding of reduced frequencies is not clear. Detailed measurements of the flow field about compliant membrane lifting surfaces are necessary to characterize the flow and its influence on the membrane dynamics.

V. Conclusions

A series of experiments were conducted to examine the effect of aspect ratio and the initial tension of a LAR compliant membrane wing. It was observed that the nearly 50% increase in the aspect ratio as compared to the wing geometry of Galvao et al. results in a portion of the wing generating lift via potential flow in the inboard region with vortex lift due to the tip vortices being confined to a region near the tip.

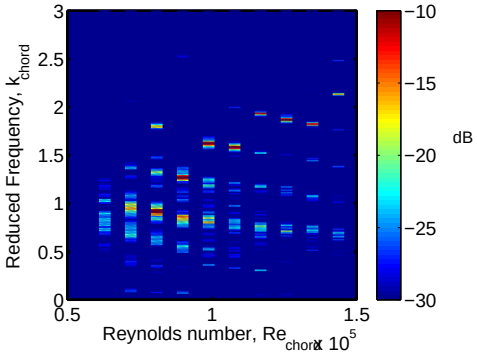

Figure 9. Waterfall chart for the membrane vibrational behavior for $\alpha = 24°$. For each Reynolds number, a power spectrum is obtained and plotted versus reduced frequency $k = fc/U$.

The cambering behavior of the LAR compliant membrane wing was observed to qualitatively follow the behavior predicted by a simple model which matches a deflection magnitude with an aerodynamic load. The decrease of the camber slope with increasing Reynolds number is seen to be a result of the combination of the small values of the deflection angle and elongation at small values of camber.

The dynamic behavior of the membrane for the aspect ratio considered is observed to be more complex than seen in the experiments of Galvao et al.[15] With very low aspect ratio wings, the influence of the tip vortices span over the entirety of the wing's surface. However, as the aspect ratio is increased the region of potential lift is increased and the region of vortex lift is decreased. This increase in the area of influence of potential lift in the inboard region of the wing appears to be manifest in the reduced magnitude of the RMS of the membrane vibration in this region. In addition, higher order spatial modes due to resonance between the membrane and flow structures are observed to occur only in a specific range of angles of attack and Reynolds number. The range of angle of attack of these higher order modes corresponds to the near stall region of the camber data suggesting that fluid-structure interaction may contribute to the softer stall characteristics of the compliant membrane wing.

Future work includes:

- Detailed measurements of the flow field about a compliant membrane wing via high speed particle image velocimetry,
- Wing geometries which more closely resemble the wings of bats.

Acknowledgements

We gratefully acknowledge the assistance of the entire Turbulence and Animal Flight Research Lab at Brown University, particularly Drs. Sharon Swartz and David Willis whose suggestions and discussions have been invaluable. This work is supported by AFOSR monitored by Drs. R. Jeffries and W. Larkin.

References

[1]Mueller, T. J. and DeLaurier, J. D., *An Overview of Micro Air Vehicle Aerodynamics*, chap. 1, AIAA, 2001, pp. 1–10.

[2]Spedding, G. R., Hedenstrom, A., and Rosen, M., "Quantitative studies of the wakes of freely flying birds in a low-turbulence wind tunnel," *Experiments in Fluids*, Vol. 34, 2003, pp. 291–303.

[3]Norberg, U. M., "Wing design, flight performance, and habitat use in bats," *Ecological morphology: integrative organismal biology*, edited by P. C. Wainwright and S. M. Reilly, University of Chicago Press, Chicago, 1994, pp. 204–239.

[4]Shyy, W., Berg, M., and Ljungqvist, D., "Flapping and flexible wings for biological and micro air vehicles," *Progress in Aerospace Sciences*, Vol. 35, No. 5, 1999, pp. 455–505.

[5]Tian, X., Iriarte-Diaz, J., Middleton, K., Galvao, R., Israeli, E., Roemer, A., Sullivan, A., Song, A., Swartz, S., and Breuer, K., "Direct measurements of the kinematics and dynamics of bat flight," *Bioinspiration & Biomimetics*, Vol. 1, 2006, pp. S10–S18.

[6]Bishop, K., "The relationship between 3-D kinematics and gliding performance in the southern flying squirrel, Glaucomys volans," *Journal of Experimental Biology*, Vol. 209, No. 4, 2006, pp. 689–701.

[7]Norberg, U. M., *Vertebrate flight: mechanics, physiology, morphology, ecology and evolution*, Springer-Verlag, Berlin, 1990.

[8]Pennycuick, C. J., "Mechanics of flight," *Avian Biology*, edited by D. S. Farner, J. R. King, and K. C. Parkes, Vol. 5, Academic Press, New York, 1975, pp. 1–75.

[9]Dickinson, M. H., Lehmann, F. O., and Chan, W. P., "The control of mechanical power in insect flight," *American Zoologist*, Vol. 38, No. 4, 1998, pp. 718–728, Times Cited: 3 Article English Cited References Count: 59 125yn.

[10]Swartz, S. M., Bishop, K. L., and Ismael-Aguirre, M.-F., "Dynamic complexity of wing form in bats: implications for flight performance," *Functional and evolutionary ecology of bats*, edited by Z. Akbar, G. McCracken, and T. H. Kunz, Oxford University Press, Oxford, 2005.

[11]Shyy, W. e. a., "Rigid and Flexible Low Reynolds Number Airfoils," *Journal of Aircraft*, Vol. 36, No. 3, 1999, pp. 523–529.

[12]Torres, G. and Mueller, T., *Aerodynamic Characteristics of Low Aspect Ratio Wings at Low Reynolds Numbers*, chap. 7, AIAA, Reston, VA, 2001, pp. 115–141.

[13]Tian, X., Israeli, E., Bishop, K., Swartz, S., and Breuer, K., "The Aerodynamics of Low Aspect Ratio Compliant Membrane Wings," Submitted to AIAA Journal.

[14]Shyy, W., Ifju, P., and Viieru, D., "Membrane Wing-Based Micro Air Vehicles," *Applied Mechanics Reviews*, Vol. 58, 2005, pp. 283–301.

[15]Galvao, R., Israeli, E., Song, A., Tian, X., Bishop, K., Swartz, S., and Breuer, K., "The Aerodynamics of Compliant Membrane Wings Modelled on Mammalian Flight Mechanics," *24th AIAA Applied Aerodynamics Conference*, 2006.

[16]Mikhail, E., Bethel, J., and McGlone, J., *Introduction to Modern Photogrammetry*, John Wiley & Sons, Inc., 2001.